Modeling the phase equilibria of asymmetric hydrocarbon mixtures using molecular simulation and equations of state

Nikolaidis, Ilias K.; Poursaeidesfahani, Ali; Csaszar, Zsolt; Ramdin, Mahinder; Vlugt, Thijs J.H.; Economou, Ioannis G.; Moultos, Othonas A.

DOI
10.1002/aic.16453

Publication date
2019

Document Version
Accepted author manuscript

Published in
AIChE Journal

Modeling the Phase Equilibria of Asymmetric Hydrocarbon Mixtures Using Molecular Simulation and Equations of State

Ilias K. Nikolaidis,[1,3] Ali Poursaeidesfahani,[2] Zsolt Csaszar,[2] Mahinder Ramdin,[2] Thijs J.H. Vlugt,[2] Ioannis G. Economou,[1,4] and Othonas A. Moultos[2,*]

[1]National Center for Scientific Research "Demokritos", Institute of Nanoscience and Nanotechnology, Molecular Thermodynamics and Modelling of Materials Laboratory, GR – 153 10 Aghia Paraskevi Attikis, Greece

[2]Delft University of Technology, Faculty of Mechanical, Maritime and Materials Engineering, Process & Energy Department, Engineering Thermodynamics, Leeghwaterstraat 39, 2628CB Delft, The Netherlands

[3]National Technical University of Athens, School of Chemical Engineering, Heroon Polytechniou Street 9, Zografou Campus, GR - 15780 Athens, Greece

[4]Texas A&M University at Qatar, Chemical Engineering Program, Education City, PO Box 23874, Doha, Qatar

[*]corresponding author: o.moultos@tudelft.nl

Abstract

Monte Carlo simulation (MC) is combined with equations of state (EoS) to develop a methodology for the calculation of the vapor – liquid equilibrium (VLE) of multicomponent hydrocarbon mixtures with high asymmetry. MC simulations are used for the calculation of the VLE of binary methane mixtures with long *n*-alkanes, for a wide range of temperatures and pressures, to obtain sufficient VLE data for the consistent fitting of binary interaction parameters (BIPs) for the EoS. The Soave-Redlich-Kwong (SRK), Peng-Robinson (PR) and PC-SAFT EoS are considered. The ability of each EoS to correlate the VLE data is assessed and the selected ones are used to predict the VLE of multicomponent gas condensate mixtures. MC simulations proved to be very accurate in predicting the VLE in all conditions and mixtures

considered. The BIPs regressed from the simulation dataset lead to equally accurate modeling results for multicomponent mixtures, compared to those regressed from experimental data.

Introduction

The significant progress and development in the drilling technology has made possible the exploitation of deep, high pressure - high temperature (HPHT) oil reservoirs for hydrocarbon production.[1] Due to the depletion of conventional resources, the oil and gas industry is driven to explore and extract petroleum fluids from geological formations and wells located in the deep crust, which differ significantly from the conventional ones with respect to temperature (T), pressure (P) and composition.[1] The temperature in such reservoirs can vary from 150 to 260 ^{o}C and the pressure from 70 to 200 MPa.[2] The fluid composition can be very asymmetric, with methane (CH_4) being the dominant component, mixed with long-chain normal alkanes (*n*-alkanes).[1,3]

The asymmetric nature of these reservoir fluids results in a more complex phase behavior, compared to those extracted from conventional wells.[3] A class of hydrocarbon mixtures that are present in HPHT reservoirs are the so-called gas condensate mixtures. The phase behavior of these systems differs from the phase behavior of conventional natural gas, because liquid can be condensed from the gas with pressure reduction at the temperature of the reservoir. As a result, the pressure decrease upon depletion of the reservoir can lead to significant loss of valuable product via liquid condensation, if precautions are not taken.[4] An important part of the gas production chain is the transportation of a methane rich stream from the point of extraction to the processing units and finally to the distribution network. The detailed

design and optimization of uninterrupted transport processes require accurate knowledge of the physical properties and the phase equilibria conditions of the hydrocarbon mixtures as functions of temperature, pressure and composition.

Experimental measurements of the physical properties and phase equilibrium of real reservoir fluids are relatively scarce. The modeling of these mixtures is a challenging task, due to the theoretical limitations in the available models and to the high uncertainties of the composition in such complex systems.[3] Current practice focuses on the experimental determination of these properties for synthetic mixtures comprised mainly of *n*-alkanes. A comprehensive review of the available experimental studies of asymmetric ternary and multicomponent hydrocarbon mixtures is given by Regueira et al.[5]

Experimental measurements for multicomponent mixtures are usually expensive and difficult to perform and do not cover the full range of working conditions. To that extent, thermodynamic models that can accurately predict the phase behavior and the physical properties of reservoir fluids are very important for the oil and gas industry, so that optimized and safe processes can be designed. Usually, the available experimental data of synthetic hydrocarbon mixtures are utilized for the assessment of existing models and the development of new ones. The agreement between model predictions and experimental data, for different mixtures, indicates how well these predictions can be extrapolated to conditions for which experimental data are not available.

To the best of our knowledge, there are two systematic research studies regarding the modeling of gas condensate mixtures. Yan et al.[6] made a comparative study between cubic such as Soave-Redlich-Kwong (SRK)[7] and Peng-Robinson (PR)[8]

and higher order (simplified PC-SAFT[9], sPC-SAFT, and Soave modified Benedict-Webb-Rubin[10], SBWR) EoS, to assess the performance of each model in predicting physical properties and phase equilibria of reservoir fluids. The authors considered density predictions of each EoS for pure components that typically exist in reservoir fluids, isothermal VLE of relevant binary mixtures, VLE predictions of synthetic multicomponent mixtures, and *PVT* properties of real reservoir fluids. It was concluded that the predictions of the four models regarding the VLE of synthetic gases are very similar, with or without the use of k_{ij} parameters, if the mixtures are not very asymmetric. Discrepancies between the models are becoming more prominent for more asymmetric mixtures, while the values of the BIPs play an important role in the accurate prediction of the phase behavior. The authors mention that the k_{ij} parameters between hydrocarbons, other than CH_4, were set equal to zero, while the most important pairs contained CH_4, N_2, CO_2 and H_2S.

In a recent study, Novak et al.[11] evaluated the performance of the SRK, PR, PC-SAFT[12] and UMR-PRU[13] models to predict dew points and liquid dropouts of synthetic and real gas condensates. The authors concluded that, in most cases, PC-SAFT predicts higher dew-point pressures than the experimentally measured ones for the synthetic gases, cubic EoS fail to describe the mixtures containing aromatic components, while the UMR-PRU model exhibits the lowest overall deviation from the experimental data. As a first step in their methodology, the authors evaluated the effect of the k_{ij} parameters on the calculations. It was shown that the use of k_{ij} parameters only between CH_4 and long-chain hydrocarbons (with 10 carbon atoms or more) yields practically the same results with those obtained when k_{ij} parameters for all binary pairs containing CH_4 are used. The exploitation of the complete matrix of

binary pairs yields also very similar results. This finding indicates that the performance of each model in predicting the VLE of these multicomponent mixtures depends mainly on specific interaction pairs of molecules, *i.e.* between CH_4 and long-chain hydrocarbons. It is important to note that the synthetic mixtures considered by Novak et al.[11] did not include N_2, CO_2 and H_2S, which would require additional k_{ij} parameters. Finally, it was emphasized that the regression of BIPs based on the respective binary mixture data is not always possible and there may be large uncertainties regarding the values of the parameters. This is a result of insufficient experimental VLE data for binary mixtures of CH_4 with long-chain hydrocarbons, especially at high pressures.

Fitting BIPs to binary mixture VLE data that do not span a wide temperature and pressure range may lead to false assessment of the correlative ability of different models. For example, even with one temperature independent k_{ij} parameter, some EoS can correlate better a wide temperature and pressure range of binary mixture VLE than others. The use of a limited number of experimental VLE data in the fitting process may result in similar performance, in terms of correlation of the phase behavior, with different thermodynamic models. The use of BIPs fitted to limited VLE data to predict the phase equilibria of multicomponent mixtures can lead to erroneous evaluation of the predictive capabilities of the models considered.

The phase equilibria of CH_4 binary mixtures with *n*-alkanes up to *n*-$C_{10}H_{22}$ are well studied in terms of experimental measurements. The mixture of CH_4 with *n*-$C_{16}H_{34}$ constitutes a very well-studied benchmark that is used also for the validation of experimental apparatuses. However, experimentally measured VLE data for mixtures with lower asymmetry, such as CH_4 - *n*-$C_{12}H_{26}$ and CH_4 - *n*-$C_{14}H_{30}$ are much

scarcer and the available experimental data do not cover the full temperature and pressure range of conditions which are encountered in multicomponent applications. In cases of mixtures with higher asymmetry, the reported experimental data are also not sufficient. Table 1 summarizes the available VLE experimental data from literature for binary CH_4 - *n*-alkane mixtures. As the asymmetry of a mixture increases, so does the temperature and pressure range where VLE is exhibited. Thus, experimental measurements have to be carried out at very high temperatures and pressures, which significantly increases the difficulty and the cost.

Molecular simulation is a powerful tool for the accurate prediction of phase equilibria and transport properties of pure components and binary mixtures.[14-17] During the past three decades, the rapid development of computers enabled the development of accurate potentials representing the intermolecular interactions and the simulation of the phase equilibria of various complex systems.[14,18] Monte Carlo simulation in the Gibbs Ensemble (GEMC) is the primary tool for calculating the phase coexistence of pure components and mixtures.[19,20] In the GEMC, two phases are simulated explicitly in two different simulation boxes without an interface. Molecules in the same simulation box interact with each other, but there are no interactions between molecules of different simulation boxes. Equilibrium is obtained by variation of the volume of each box and molecule exchange between the boxes. Although GEMC provides a straightforward route to determine accurate coexistence densities, the computation of critical parameters is not always easy.[21] To that end, alternative simulation methods such as the histogram reweighting in the grand-canonical ensemble,[22,23] the Gibbs-Duhem integration technique[24,25] and the iterative Monte Carlo scheme[26] (SPECS) can be very efficient, provided that the number of components is limited and the acceptance probability for insertions/deletions of

molecules is sufficiently high. Nevertheless, GEMC combined with advanced techniques such as the configurational-bias Monte Carlo (CBMC)[27-29] or continuous fractional component Monte Carlo (CFCMC)[30-33], which increase the acceptance probability of the molecule exchange trial move, is still a very reliable and efficient tool for the phase equilibria calculation of hydrocarbon mixtures.

The aim of this work is to develop a methodology for the prediction of the VLE of multicomponent gas condensate mixtures by combining molecular simulation with thermodynamic models in the form of an EoS. Monte Carlo simulations in the Gibbs Ensemble with the TraPPE-UA force field[15] are used for the calculation of VLE data for various binary CH_4 - *n*-alkane mixtures. In total, 5 binary mixtures are investigated: the mixtures of CH_4 with *n*-$C_{10}H_{22}$, *n*-$C_{12}H_{26}$, *n*-$C_{16}H_{34}$, *n*-$C_{20}H_{42}$ and *n*-$C_{24}H_{50}$. Initially, the GEMC simulation results are validated against the available experimental data and subsequently new calculations are performed at conditions in which no experimental measurements exist. Two sets of k_{ij} parameters for two cubic (SRK, PR) and one higher order (PC-SAFT) EoS are then regressed; one from the available experimental VLE data for the 5 binary mixtures and a second one using the GEMC simulation results. The aim is to compare the variation of the k_{ij} values when fitted to experimental data at the available range of conditions versus the respective k_{ij} values fitted to GEMC simulation data which span an extensive temperature and pressure range. The ability of each EoS to correlate the VLE data depending on the available range of conditions is also assessed. Finally, the EoS considered in this work are used to predict the VLE of multicomponent gas condensate mixtures with both sets of k_{ij} parameters and a comparison between the models is performed. The gas condensate mixtures considered in this study consist mainly of *n*-alkanes. Although

multicomponent mixtures including components like CO_2 and N_2, or even sour gases with high concentration of H_2S (and / or CO_2), better resemble reservoir fluids, the scope of this work is to concentrate on mixtures of alkanes, only. For the five binary CH_4 - *n*-alkanes mixtures studied in this work, an extensive number of MC simulations is required to cover the wide range of temperatures and pressures for the accurate prediction. The consideration of CO_2, N_2 and H_2S would require a significant number of additional MC simulations to validate and extend the binary mixture data. In addition, molecular simulation studies of hydrocarbons with polar molecules often require modifications of the binary interaction parameters used, mainly due to deficiencies in the force fields of the polar components.[34-39] This study will be the focus of a future work.

Models and Methods

Equations of State

An EoS is a mathematical relation that correlates the temperature, pressure, and molar volume (v) of a pure component at a thermodynamic equilibrium state. According to the Gibbs phase rule for a single-phase pure component, the EoS can be solved for one of these quantities while the other two are set.[40] The usual case is that the EoS is solved for the volume, at constant temperature and pressure, and then all other thermodynamic properties can be determined, using specific thermodynamic relations. The most well-known EoS are the SRK and PR which belong to the family of cubic EoS (cubic dependency on volume) and are empirical modifications of the pioneering van der Waals EoS.[41] Mixture properties can be calculated by a cubic EoS using appropriate combining and mixing rules. In this work, the SRK and PR EoS

were applied to mixtures via the van der Waals one fluid theory (vdW1f) mixing rules, using only one temperature-independent BIP (k_{ij}) in the attractive term.

SAFT based models are theoretically derived EoS based on rigorous perturbation theory.[42-44] A SAFT model that has gained tremendous industrial popularity is the PC-SAFT EoS.[12] PC-SAFT was derived using the hard chain fluid as the reference system and the second order Barker – Henderson (BH) perturbation theory[45] was applied for the Helmholtz free energy term that accounts for the dispersion interactions. The pair potential used is the modified square well potential, proposed by Chen and Kreglewski.[46] The chain and association terms in PC-SAFT EoS are the same as the ones used in the SAFT EoS proposed by Huang and Radosz.[47,48] The reader can refer to the original publications[12,49] for the exact mathematical relations. In this work, the PC-SAFT EoS was used to calculate mixture properties with the vdW1f mixing rules as proposed by Gross and Sadowski,[12] while specific combining rules (Lorentz – Berthelot-based with a BIP incorporated into the Berthelot rule) were applied to calculate the segment dispersive energy and diameter parameters for the unlike interactions. More details on the Cubic and PC-SAFT EoS are provided in the Supporting Information.

Monte Carlo Simulation

Monte Carlo simulations were performed in the Gibbs-NPT ensemble to compute the VLE of mixtures.[14,19,20] In the Gibbs-NPT ensemble, the volume of the two boxes can be changed independently and different kinds of MC moves are performed to satisfy the equilibrium conditions, *i.e.*, the equality of temperature, pressure, and chemical potential of each component in the coexisting phases. In each MC step, a trial move is selected at random to displace, regrow, rotate or exchange a

chosen hydrocarbon chain or change the volume of a randomly selected box. GEMC relies on a sufficient number of molecule exchanges between the simulation boxes. Unfortunately, the acceptance probabilities for these exchanges can be close to zero for the case of long molecules or when densities are high (*e.g.*, a liquid phase at low temperature).

Although GEMC has been used to study a wide range of mixtures, simulation data for asymmetric mixtures of hydrocarbons are scarce. This should be attributed, among others, to the low acceptance probability for the exchange of the long-chain hydrocarbons. At these conditions, advanced simulation techniques such as CBMC[27-29] or CFCMC[30,31] are used to increase the acceptance probability of the molecule exchange trial move. Details for these simulation techniques are given in the Supporting Information. In this work, all simulations were performed using the CBMC method, while the CFCMC method was used to verify the results for systems where the exchange of molecules between the boxes is expected to be more difficult (e.g. CH_4 - *n*-$C_{20}H_{42}$ and CH_4 - *n*-$C_{24}H_{50}$ at low temperatures and high pressures).

In this work, the TraPPE united atom (TraPPE-UA) force field was used for all the *n*-alkanes.[15] In the TraPPE-UA, CH_4, CH_3 and CH_2 groups are modeled as pseudo-atoms with no charges. The non-bonded intra- and intermolecular interactions between the pseudo-atoms are represented by the 12-6 Lennard-Jones (LJ) potential. The LJ parameters used in this study can be found in the work by Martin and Siepmann.[15] Force field and computational details for the MC simulations are given in the Supporting Information. All GEMC simulations were carried out with RASPA.[50,51]

Results and Discussion

Monte Carlo Simulations

The computed VLE from the GEMC simulations depends heavily on the accuracy of the force fields used. As mentioned in the previous section, TraPPE-UA was used in all our simulations. The choice of this force field was based on various reasons: Siepmann and coworkers reported the VLE of pure alkanes up to *n*-$C_{12}H_{26}$,[15] showing that the TraPPE-UA force field is sufficiently accurate in reproducing the VLE of these hydrocarbons. In addition, the use of united atom force fields is advantageous due to the significant reduction of interaction sites compared to their full atom counterparts (e.g., TraPPE-EH[52]). One of the drawbacks of the TraPPE-UA force field is the tendency to slightly overestimate the vapor pressures and densities.[15] However, the saturated liquid densities and critical temperatures are predicted accurately.[15] Therefore, since the liquid phase properties at high temperatures are represented well by the TraPPE-UA force field, it is expected that the k_{ij} parameters, which are typically fitted to bubble-point data, will not be affected by the deficiency of the model to accurately describe the gas-phase.

To validate the TraPPE-UA force field, the VLE of binary mixtures of CH_4 with different long-chain *n*-alkanes were computed in the Gibbs-NPT ensemble and compared with available experimental data. In Figure 1, the simulated VLE data for the most asymmetric mixture (i.e., CH_4 - *n*-$C_{24}H_{50}$) at temperatures ranging from 330 K to 523.15 K are plotted against the available experimental data. Excellent agreement between the two sets of data is observed, even at conditions close to the critical points. Similarly, good agreement is observed for all the mixtures considered, justifying the choice of the TraPPE-UA force field. Relevant comparisons between

experiments and simulations can be found in the Supporting Information (Figures S1 through S5).

Equation of State Modeling

The accurate phase equilibrium modeling of asymmetric hydrocarbon mixtures with EoS relies heavily on the BIPs between CH_4 and long-chain hydrocarbons.[11] In this work, temperature independent k_{ij} parameters are used in the combining rules of the adopted EoS. A different model selection would require the use of different BIPs, *e.g.*, energetic interactions in Excess Gibbs Energy models, interactions between groups in group contribution schemes, etc.[53-55] Except for the thermodynamic model itself, the number of BIPs, their temperature dependency, etc. affects the general correlative ability of the model.

Tables S1 and S2 summarize the pure component parameters used for the cubic and PC-SAFT EoS respectively. The critical properties and the acentric factor for the cubic EoS were taken from the DIPPR[56] database, while the PC-SAFT EoS parameters were taken from Gross and Sadowski,[12] except for the *n*-$C_{24}H_{50}$ parameters, which were taken from the MAPS platform v4.0.[57]

Comparison of Calculations from the Various Methods

A major aim in this work is to evaluate k_{ij} parameters by fitting the EoS to GEMC simulation data generated here, and to experimental data available in the literature. As shown in the previous section, GEMC simulations can provide accurate VLE predictions for the binary mixtures considered. In this work, GEMC simulations were also performed at conditions where no experimental data are available. The aim was to cover the entire temperature range from the normal melting temperature to the

critical temperature of the long-chain *n*-alkane in every mixture. We aim to show that molecular simulation based on accurate force fields is a powerful tool that can be used to complement experiments and provide useful insight at conditions in which measurements are difficult to be carried out (e.g., high temperature and pressures). The pressure range examined in the simulations spans from low values up to approximately the binary mixture critical point. To avoid conditions where solidification may occur, the lowest isotherm is approximately 10 K higher than the normal melting point and the highest one is approximately 50 K lower than the critical temperature of the long-chain *n*-alkane, respectively.

In this work, two sets of k_{ij} parameters were obtained: One by minimizing the root-mean-square deviation between the bubble pressure values calculated by the EoS and experimental data and the second one by minimizing the same deviation between EoS calculations and GEMC data. Table 2 summarizes the Percentage Average Absolute Relative Deviation (% AARD) between experimental VLE data and EoS calculations for each mixture and the corresponding k_{ij} values. Table 3 summarizes the % AARD and the respective k_{ij} values for the case where GEMC simulation VLE data were used. In the rest of the paper, the % AARD and k_{ij} parameters calculated from the experimental VLE data will be referred to as % AARD-EXP and k_{ij}^{EXP}, while those calculated from GEMC simulations as % AARD-MC and k_{ij}^{MC}, respectively. As a general trend, it should be pointed out that the k_{ij} values are relatively small in all cases, and EoS predictions are in reasonable agreement with both experimental and GEMC data, even when $k_{ij} = 0$. An assessment of these calculations is shown in Tables 2 and 3.

In Figure 2, the variation of % AARD-EXP and % AARD-MC with the carbon number of the long-chain *n*-alkane in each binary mixture is presented. All the binary mixtures considered in this work include only *n*-alkanes and one might expect that the % AARD will increase as the asymmetry of each mixture increases, *i.e.*, with the carbon number. However, this is not always the case here. The two cubic EoS essentially deviate from the expected behavior because of the % AARD-EXP value of CH_4 - *n*-$C_{16}H_{34}$ mixture, which has a lower value compared to CH_4 - *n*-$C_{12}H_{26}$ mixture. The most prevalent deviation from the expected behavior is presented by PC-SAFT EoS which correlates with almost the same accuracy in terms of % AARD-EXP values (approximately 5.3%) the VLE of CH_4 mixtures with *n*-$C_{10}H_{22}$, *n*-$C_{12}H_{26}$, *n*-$C_{20}H_{42}$ and *n*-$C_{24}H_{50}$. A distinctively higher value (% AARD-EXP = 8.47) is presented for the CH_4 - *n*-$C_{16}H_{34}$ mixture. The relative constant k_{ij} can be attributed partly to the strong theoretical basis of PC-SAFT that captures accurately the properties of long hydrocarbon molecules.

The same trend presented for the % AARD-EXP of the cubic EoS in this work is also followed by the respective values reported by Yan et al.[6], while the absolute values are also similar. The k_{ij}^{EXP} values regressed in this work are in very good agreement with those reported by Novak et al.[11] that also used the DIPPR[56] database for the pure component parameters of the cubic EoS and the Gross and Sadowski[12] ones for PC-SAFT. Taking into account the possible differences in tolerance values for the fitting of BIPs, the calculation procedure for the VLE and the exact experimental data used by the various authors, it can be assessed that the agreement with prior work is sufficiently good.

As it can be observed from Figure 2(b), the % AARD-MC for all three EoS always increases with the carbon number, following the expected behavior. The three EoS present similar % AARD-MC values for the mixtures of CH_4 with *n*-$C_{10}H_{22}$, *n*-$C_{16}H_{34}$ and *n*-$C_{20}H_{42}$, while PC-SAFT presents two distinct values for the CH_4 - *n*-$C_{12}H_{26}$ and CH_4 - *n*-$C_{24}H_{50}$ mixtures when compared to the cubic EoS. The two cubic EoS present very similar % AARD-MC values for all the binary mixtures considered. Comparing the % AARD-MC values to the respective % AARD-EXP, it is observed that the CH_4 - *n*-$C_{10}H_{22}$ value remains almost constant for the cubic EoS, while others change significantly resulting in a totally different assessment between the three models. A more detailed analysis for each mixture and the correlative ability of the EoS considered is presented below.

Figures 3 through 7 refer to P-xy phase diagrams for the binary mixtures considered at various temperatures, with the three EoS using k_{ij} parameters regressed from GEMC simulation data. Experimental and GEMC simulation data are plotted together (when available) at the selected temperatures, showing the very good agreement between the two datasets. Figure 3 shows the P-xy diagrams for the CH_4 - *n*-$C_{10}H_{22}$ mixture at temperatures from 244.26 to 583.05 K. All EoS correlate accurately the two datasets with the % AARD-MC being almost equal for the cubic and PC-SAFT. Furthermore, the % AARD-EXP for the cubic EoS is similar to % AARD-MC, while a higher difference is presented for PC-SAFT. This higher variation of the % AARD value for PC-SAFT is attributed to the VLE data at 244.26 K. The k_{ij} parameters of PC-SAFT EoS generally show higher sensitivity to the dataset used for the regression, compared to the respective ones of cubic EoS.[6,58] However, similar sensitivity of the k_{ij} parameters for the three EoS is shown when high temperature VLE GEMC simulation data are added. This indicates that the

higher sensitivity of the BIPs of PC-SAFT may be attributed mainly to the low temperature VLE correlation.

In Figure 4, the VLE correlation results for the CH_4 - *n*-$C_{12}H_{26}$ mixture are presented with the three EoS. The isotherms at 303.15 and 373.2 K are correlated almost with the same accuracy by the three EoS. At higher temperatures (450 and 550 K), cubic EoS correlate slightly more accurately the equilibrium pressure away from the critical point compared to PC-SAFT, in expense of a more significant critical point over prediction. It is prevalent even at 373.2 K, that SRK presents the most significant over prediction of the critical point, with PR following and with PC-SAFT being the most accurate. Comparing the % AARD-EXP and % AARD-MC values for this mixture, it can be assessed that the addition of high-temperature VLE data for the regression shifts the % AARD to lower values for the cubic EoS, since they are more successful in correlating the high temperature VLE and to a higher value for PC-SAFT which correlates better the low temperature data. Note that the available experimental VLE data for this mixture are in the range of 263.15 - 373.2 K, while the critical temperature of *n*-$C_{12}H_{26}$ is 650 K. GEMC simulations were performed at isotherms from 283 to 600 K to obtain a wider range of pseudo-experimental data for CH_4 - *n*-$C_{12}H_{26}$. Results are plotted in Figure 5 for the CH_4 - *n*-$C_{16}H_{34}$ mixture with calculations from the three EoS and k_{ij}^{MC}. In this case, the difference between the three EoS in the critical point prediction becomes even more pronounced with the increase of temperature.

Figures 6 and 7 show the VLE results for the mixtures of CH_4 with *n*-$C_{20}H_{42}$ and *n*-$C_{24}H_{50}$. For these two mixtures, the improved correlation of the VLE behavior at low temperatures (323.15 and 330 K respectively) with PC-SAFT EoS is more

pronounced. At high temperatures, especially from 500 K and higher, cubic EoS correlate more accurately the equilibrium pressure than PC-SAFT. As with the previous mixtures, SRK EoS predicts the highest critical pressures, while PC-SAFT EoS predicts the lowest ones. At temperatures close to the normal melting temperature of the long-chain *n*-alkane of every mixture, the two cubic EoS predict almost the same critical pressure. The experimental data for the CH_4 - *n*-$C_{20}H_{42}$ mixture span from 323.15 to 573.15 K, while GEMC simulation data cover a temperature range from 323 to 700 K. The respective range for the CH_4 - *n*-$C_{24}H_{50}$ mixture is 330 - 573.15 K for the experiments and 330 - 750 K for the GEMC simulation data.

The two sets of k_{ij} parameters were used for the calculation of constant composition VLE of asymmetric multicomponent mixtures, comprised mainly of *n*-alkanes. The compositions of the mixtures studied are summarized in Table 4. The k_{ij} parameters between CH_4 and alkanes with lower molecular weight than *n*-$C_{10}H_{22}$ were taken from Novak et al.[11] Alternatively the interaction parameter values for these binary pairs could have been set equal to zero and almost the same modeling results would have been obtained, since their effect is negligible, as shown by Novak et al.

In Figure 8, the results for the multicomponent mixtures considered are presented, with the two cubic and PC-SAFT EoS. The difference between calculations with the two sets of k_{ij} parameters is practically negligible. The highest deviations between the two sets of calculations are presented with PC-SAFT EoS for the synthetic gas condensates (SGCs) 4, 5, 6 and 7. For SGC4, the deviations in the calculated equilibrium pressure start close to 280 K and are approximately 1 MPa. For

SGCs 5, 6 and 7 the deviations appear close to 290 K and vary from 1 to 2.5 MPa. Both cubic EoS are much more insensitive to the choice of the set of k_{ij} parameters for the mixtures mentioned. Very low sensitivity to the choice of BIPs is manifested in SGC3 mixture with all three EoS. It should be noticed that the composition of SGC3 in terms of high molecular weight *n*-alkanes is higher compared to SGC4. This results in the equilibrium measurements being bubble points instead of dew points, as opposed to all the other mixtures studied. This is the only mixture in which PC-SAFT EoS is clearly more accurate than the cubic ones.

Conclusions

A predictive methodology was developed for the calculation of the VLE of multicomponent hydrocarbon mixtures with high asymmetry, combining molecular simulations and EoS. MC simulations in the Gibbs Ensemble were used for the calculation of the VLE of binary CH_4 mixtures with *n*-alkanes, to be used as a pseudo-experimental dataset, for a consistent fitting of the BIPs of the thermodynamic models. Two cubic (SRK, PR) and one higher order (PC-SAFT) EoS were used to correlate the binary-mixture VLE data and subsequently predict the multicomponent mixture VLE. GEMC simulations with the TraPPE-UA force field were validated with experimental VLE data for the binary mixtures considered. It was shown that accurate predictions can be retrieved even in very asymmetric mixtures. It is assessed that GEMC simulations can be carried out with high accuracy at temperatures and pressures in which no experimental VLE data exist, thus covering a wide range of conditions, suitable for fitting BIPs of thermodynamic models. k_{ij} parameters with the three EoS were regressed from both experimental and GEMC simulation data. It is shown that the use of a dataset that spans a wide range of temperatures and pressures

consistently affects the k_{ij} values. It is also observed that for the CH_4 - n-$C_{10}H_{22}$ mixture the three EoS correlate with equal accuracy the VLE behavior, while with increasing asymmetry, PC-SAFT EoS is more successful in correlating the low temperature data and cubic EoS the high temperature data. Finally, the BIPs regressed from GEMC simulation data lead to equally accurate modeling results for multicomponent mixtures, compared to those regressed from experimental binary mixture data. Consequently, molecular simulations using accurate force fields can be used to generate precise VLE data for binary mixtures of CH_4 with n-alkanes, in the absence of experimental data.

Associated Content

EoS and MC details; Critical temperature, pressure and acentric factor data; PC-SAFT EoS parameters; GEMC simulation data; comparison of GEMC and experimental data.

Acknowledgments

This research has been funded by the General Secretariat for Research and Technology (GSRT) and the Hellenic Foundation for Research and Innovation (HFRI). The work at Delft University of Technology was sponsored by NWO Exacte Wetenschappen (Physical Sciences) for the use of supercomputer facilities with financial support from the Nederlandse Organisatie voor weten schappelijk Onderzoek (Netherlands Organization for Scientific Research, NWO). TJHV acknowledges NOW-CW for a VICI grant. The statements made herein are solely the responsibility of the authors.

References

1. Machado JJB, de Loos TW. Liquid–vapour and solid–fluid equilibria for the system methane + triacontane at high temperature and high pressure. Fluid Phase Equilibria. 2004;222–223:261-267.
2. Schlumberger. *High-Pressure, High-Temperature Technologies* 10/01/2008 2008.
3. Ungerer P, Faissat B, Leibovici C, et al. High pressure-high temperature reservoir fluids: investigation of synthetic condensate gases containing a solid hydrocarbon. Fluid Phase Equilibria. 1995;111:287-311.
4. Shariati A, Straver EJM, Florusse LJ, Peters CJ. Experimental phase behavior study of a five-component model gas condensate. Fluid Phase Equilibria. 2014;362:147-150.
5. Regueira T, Liu Y, Wibowo AA, et al. High pressure phase equilibrium of ternary and multicomponent alkane mixtures in the temperature range from (283 to 473) K. Fluid Phase Equilibria. 2017;449:186-196.
6. Yan W, Varzandeh F, Stenby EH. PVT modeling of reservoir fluids using PC-SAFT EoS and Soave-BWR EoS. Fluid Phase Equilibria. 2015;386:96-124.
7. Soave G. Equilibrium constants from a modified Redlich-Kwong equation of state. Chemical Engineering Science. 1972;27:1197-1203.
8. Peng D-Y, Robinson DB. A New Two-Constant Equation of State. Industrial & Engineering Chemistry Fundamentals. 1976;15:59-64.
9. von Solms N, Michelsen ML, Kontogeorgis GM. Computational and Physical Performance of a Modified PC-SAFT Equation of State for Highly Asymmetric and Associating Mixtures. Industrial & Engineering Chemistry Research. 2003;42:1098-1105.
10. Soave GS. An effective modification of the Benedict–Webb–Rubin equation of state. Fluid Phase Equilibria. 1999;164:157-172.
11. Novak N, Louli V, Skouras S, Voutsas E. Prediction of dew points and liquid dropouts of gas condensate mixtures. Fluid Phase Equilibria. 2018;457:62-73.
12. Gross J, Sadowski G. Perturbed-Chain SAFT: An Equation of State Based on a Perturbation Theory for Chain Molecules. Industrial & Engineering Chemistry Research. 2001;40:1244-1260.
13. Voutsas E, Louli V, Boukouvalas C, Magoulas K, Tassios D. Thermodynamic property calculations with the universal mixing rule for EoS/GE models: Results with the Peng–Robinson EoS and a UNIFAC model. Fluid Phase Equilibria. 2006;241:216-228.
14. Frenkel D, Smit B. Understanding molecular simulation: from algorithms to applications (2nd edition). San Diego, California: Academic Press, 2002.
15. Martin MG, Siepmann JI. Transferable Potentials for Phase Equilibria. 1. United-Atom Description of n-Alkanes. The Journal of Physical Chemistry B. 1998;102:2569-2577.
16. Michalis VK, Moultos OA, Tsimpanogiannis IN, Economou IG. Molecular dynamics simulations of the diffusion coefficients of light n-alkanes in water over a wide range of temperature and pressure. Fluid Phase Equilibria. 2016;407:236-242.
17. Moultos OA, Tsimpanogiannis IN, Panagiotopoulos AZ, Trusler JPM, Economou IG. Atomistic Molecular Dynamics Simulations of Carbon Dioxide Diffusivity in n-Hexane, n-Decane, n-Hexadecane, Cyclohexane, and Squalane. The Journal of Physical Chemistry B. 2016;120:12890-12900.
18. Allen MP, Tildesley DJ. Computer simulation of liquids New York: Oxford University Press, 1989.
19. Panagiotopoulos AZ. Direct Determination of Fluid Phase Equilibria by Simulation in the Gibbs Ensemble: A Review. Molecular Simulation. 1992;9:1-23.
20. Panagiotopoulos AZ. Molecular simulation of phase equilibria: simple, ionic and polymeric fluids. Fluid Phase Equilibria. 1992;76:97-112.
21. Dinpajooh M, Bai P, Allan DA, Siepmann JI. Accurate and precise determination of critical properties from Gibbs ensemble Monte Carlo simulations. The Journal of Chemical Physics. 2015;143:114113.
22. Ferrenberg AM, Swendsen RH. New Monte Carlo Technique for Studying Phase Transitions. Physical Review Letters. 1989;63:1658-1658.

23. Rane KS, Murali S, Errington JR. Monte Carlo Simulation Methods for Computing Liquid–Vapor Saturation Properties of Model Systems. Journal of Chemical Theory and Computation. 2013;9:2552-2566.
24. Kofke DA. Gibbs-Duhem integration: a new method for direct evaluation of phase coexistence by molecular simulation. Molecular Physics. 1993;78:1331-1336.
25. Mehta M, Kofke DA. Coexistence diagrams of mixtures by molecular simulation. Chemical Engineering Science. 1994;49:2633-2645.
26. Spyriouni T, Economou IG, Theodorou DN. Phase Equilibria of Mixtures Containing Chain Molecules Predicted through a Novel Simulation Scheme. Physical Review Letters. 1998;80:4466-4469.
27. Consta S, Vlugt TJH, Hoeth JW, Smit B, Frenkel D. Recoil growth algorithm for chain molecules with continuous interactions. Molecular Physics. 1999;97:1243-1254.
28. Siepmann JI. A method for the direct calculation of chemical potentials for dense chain systems. Molecular Physics. 1990;70:1145-1158.
29. Siepmann JI, Karaborni S, Smit B. Vapor-liquid equilibria of model alkanes. Journal of the American Chemical Society. 1993;115:6454-6455.
30. Shi W, Maginn EJ. Continuous Fractional Component Monte Carlo: An Adaptive Biasing Method for Open System Atomistic Simulations. Journal of Chemical Theory and Computation. 2007;3:1451-1463.
31. Shi W, Maginn EJ. Improvement in molecule exchange efficiency in Gibbs ensemble Monte Carlo: Development and implementation of the continuous fractional component move. Journal of Computational Chemistry. 2008;29:2520-2530.
32. Poursaeidesfahani A, Hens R, Rahbari A, Ramdin M, Dubbeldam D, Vlugt TJH. Efficient Application of Continuous Fractional Component Monte Carlo in the Reaction Ensemble. Journal of Chemical Theory and Computation. 2017;13:4452-4466.
33. Poursaeidesfahani A, Torres-Knoop A, Dubbeldam D, Vlugt TJH. Direct Free Energy Calculation in the Continuous Fractional Component Gibbs Ensemble. Journal of Chemical Theory and Computation. 2016;12:1481-1490.
34. Potoff JJ, Errington JR, Panagiotopoulos AZ. Molecular simulation of phase equilibria for mixtures of polar and non-polar components. Molecular Physics. 1999;97:1073-1083.
35. Vrabec J, Fischer J. Vapor–liquid equilibria of the ternary mixture CH4 + C2H6 + CO2 from molecular simulation. AIChE Journal. 1997;43:212-217.
36. Delhommelle J, Boutin A, Fuchs AH. Molecular Simulation of Vapour-Liquid Coexistence Curves for Hydrogen Sulfide-Alkane and Carbon Dioxide-Alkane Mixtures. Molecular Simulation. 1999;22:351-368.
37. Neubauer B, Tavitian B, Boutin A, Ungerer P. Molecular simulations on volumetric properties of natural gas1Partly presented at the CECAM (Centre Européen de Calcul Atomique et Moléculaire) workshop, Lyon, France, April 26–28, 1998.1. Fluid Phase Equilibria. 1999;161:45-62.
38. Ungerer P, Nieto-Draghi C, Lachet V, et al. Molecular simulation applied to fluid properties in the oil and gas industry. Molecular Simulation. 2007;33:287-304.
39. Ungerer P, Nieto-Draghi C, Rousseau B, Ahunbay G, Lachet V. Molecular simulation of the thermophysical properties of fluids: From understanding toward quantitative predictions. Journal of Molecular Liquids. 2007;134:71-89.
40. Nikolaidis IK, Franco LFM, Vechot LN, Economou IG. Modeling of physical properties and vapor – liquid equilibrium of ethylene and ethylene mixtures with equations of state. Fluid Phase Equilibria. 2018;470:149-163.
41. Van der Waals JD. *On the continuity of the gas and liquid state* [PhD Thesis], Leiden; 1873.
42. Chapman WG, Gubbins KE, Jackson G, Radosz M. New reference equation of state for associating liquids. Industrial & Engineering Chemistry Research. 1990;29:1709-1721.
43. Chapman WG, Jackson G, Gubbins KE. Phase equilibria of associating fluids. Molecular Physics. 1988;65:1057-1079.
44. Jackson G, Chapman WG, Gubbins KE. Phase equilibria of associating fluids. Molecular Physics. 1988;65:1-31.

45. Barker JA, Henderson D. Perturbation Theory and Equation of State for Fluids. II. A Successful Theory of Liquids. The Journal of Chemical Physics. 1967;47:4714-4721.
46. Chen SS, Kreglewski A. Applications of the Augmented van der Waals Theory of Fluids.: I. Pure Fluids. Berichte der Bunsengesellschaft für physikalische Chemie. 1977;81:1048-1052.
47. Huang SH, Radosz M. Equation of state for small, large, polydisperse, and associating molecules. Industrial & Engineering Chemistry Research. 1990;29:2284-2294.
48. Huang SH, Radosz M. Equation of state for small, large, polydisperse, and associating molecules: extension to fluid mixtures. Industrial & Engineering Chemistry Research. 1991;30:1994-2005.
49. Gross J, Sadowski G. Application of the Perturbed-Chain SAFT Equation of State to Associating Systems. Industrial & Engineering Chemistry Research. 2002;41:5510-5515.
50. Dubbeldam D, Calero S, Ellis DE, Snurr RQ. RASPA: molecular simulation software for adsorption and diffusion in flexible nanoporous materials. Molecular Simulation. 2016;42:81-101.
51. Dubbeldam D, Torres-Knoop A, Walton KS. On the inner workings of Monte Carlo codes. Molecular Simulation. 2013;39:1253-1292.
52. Chen B, Siepmann JI. Transferable Potentials for Phase Equilibria. 3. Explicit-Hydrogen Description of Normal Alkanes. The Journal of Physical Chemistry B. 1999;103:5370-5379.
53. Abrams DS, Prausnitz JM. Statistical thermodynamics of liquid mixtures: A new expression for the excess Gibbs energy of partly or completely miscible systems. AIChE Journal. 1975;21:116-128.
54. Gmehling J, Rasmussen P, Fredenslund A. Vapor-liquid equilibriums by UNIFAC group contribution. Revision and extension. 2. Industrial & Engineering Chemistry Process Design and Development. 1982;21:118-127.
55. Jaubert J-N, Mutelet F. VLE predictions with the Peng–Robinson equation of state and temperature dependent kij calculated through a group contribution method. Fluid Phase Equilibria. 2004;224:285-304.
56. DIPPR 801, Evaluated Standards Thermophysical Property Values. American Institute of Chemical Engineers; 2015.
57. MAPS; Materials and Processes Simiulations Platform, Version v4.0, Scienomics. SARL, Paris, France.
58. Perez AG, Coquelet C, Paricaud P, Chapoy A. Comparative study of vapour-liquid equilibrium and density modelling of mixtures related to carbon capture and storage with the SRK, PR, PC-SAFT and SAFT-VR Mie equations of state for industrial uses. Fluid Phase Equilibria. 2017;440:19-35.
59. Koonce KT, Kobayashi R. A Method for Determining the Solubility of Gases in Relatively Nonvolatile Liquids: Solubility of Methane in n-Decane. Journal of Chemical & Engineering Data. 1964;9:490-494.
60. Rijkers MPWM, Malais M, Peters CJ, de Swaan Arons J. Measurements on the phase behavior of binary hydrocarbon mixtures for modelling the condensation behavior of natural gas: Part I. The system methane + decane. Fluid Phase Equilibria. 1992;71:143-168.
61. Srivastan S, Darwish NA, Gasem KAM, Robinson RL. Solubility of methane in hexane, decane, and dodecane at temperatures from 311 to 423 K and pressures to 10.4 MPa. Journal of Chemical & Engineering Data. 1992;37:516-520.
62. Lin H-M, Sebastian HM, Simnick JJ, Chao K-C. Gas-liquid equilibrium in binary mixtures of methane with N-decane, benzene, and toluene. Journal of Chemical & Engineering Data. 1979;24:146-149.
63. Beaudoin JM, Kohn JP. Multiphase and volumetric equilibria of the methane-n-decane binary system at temperatures between -36.degree. and 150.degree. Journal of Chemical & Engineering Data. 1967;12:189-191.
64. Reamer HH, Olds RH, Sage BH, Lacey WN. Phase Equilibria in Hydrocarbon Systems. Industrial & Engineering Chemistry. 1942;34:1526-1531.

65. Regueira T, Pantelide G, Yan W, Stenby EH. Density and phase equilibrium of the binary system methane + n-decane under high temperatures and pressures. Fluid Phase Equilibria. 2016;428:48-61.
66. Rijkers MPWM, Maduro VB, Peters CJ, de Swaan Arons J. Measurements on the phase behavior of binary mixtures for modeling the condensation behavior of natural gas: Part II. The system methane + dodecane. Fluid Phase Equilibria. 1992;72:309-324.
67. Arnaud J-F. *Caractérisation des propriétés physiques et thermodynamiques des fluides pétroliers à haute pression*, Thése de doctorat en Physique, Pau, France, 1995.
68. Glaser M, Peters CJ, Van Der Kooi HJ, Lichtenthaler RN. Phase equilibria of (methane + n-hexadecane) and (p, Vm, T) of n-hexadecane. The Journal of Chemical Thermodynamics. 1985;17:803-815.
69. Rijkers MPWM, Peters CJ, de Swaan Arons J. Measurements on the phase behavior of binary mixtures for modeling the condensation behavior of natural gas: Part III. The system methane + hexadecane. Fluid Phase Equilibria. 1993;85:335-345.
70. Siqueira Campos CEP, Penello JR, Pellegrini Pessoa FL, Cohen Uller AM. Experimental Measurement and Thermodynamic Modeling for the Solubility of Methane in Water and Hexadecane. Journal of Chemical & Engineering Data. 2010;55:2576-2580.
71. Le Roy S, Behar E, Ungerer P. Vapour-liquid equilibrium data for synthetic hydrocarbon mixtures. Application to modelling of migration from source to reservoir rocks. Fluid Phase Equilibria. 1997;135:63-82.
72. Lin H-M, Sebastian HM, Chao K-C. Gas-liquid equilibrium in hydrogen + n-hexadecane and methane + n-hexadecane at elevated temperatures and pressures. Journal of Chemical & Engineering Data. 1980;25:252-254.
73. Cohen A, Richon D. New apparatus for simultaneous determination of phase equilibria and rheological properties of fluids at high pressures: Its application to coal pastes studies up to 773 K and 30 MPa. Review of Scientific Instruments. 1986;57:1192-1195.
74. Puri S, Kohn JP. Solid-liquid-vapor equilibrium in the methane-n-eicosane and ethane-n-eicosane binary systems. Journal of Chemical & Engineering Data. 1970;15:372-374.
75. Darwish NA, Fathikalajahi J, Gasem KAM, Robinson RL. Solubility of methane in heavy normal paraffins at temperatures from 323 to 423 K and pressures to 10.7 MPa. Journal of Chemical & Engineering Data. 1993;38:44-48.
76. van der Kooi HJ, Flöter E, Loos TWd. High-pressure phase equilibria of {(1−x)CH4+xCH3(CH2)18CH3}. The Journal of Chemical Thermodynamics. 1995;27:847-861.
77. Huang SH, Lin HM, Chao KC. Solubility of carbon dioxide, methane, and ethane in n-eicosane. Journal of Chemical & Engineering Data. 1988;33:145-147.
78. Flöter E, de Loos TW, de Swaan Arons J. High pressure solid-fluid and vapour-liquid equilibria in the system (methane + tetracosane). Fluid Phase Equilibria. 1997;127:129-146.
79. Huang C-P, Jan D-S, Tsai F-N. Modeling of Methane Solubility in Heavy n-Paraffins. Journal of Chemical Engineering of Japan. 1992;25:182-186.
80. Arnaud JF, Ungerer P, Behar E, Moracchini G, Sanchez J. Excess volumes and saturation pressures for the system methane + n-tetracosane at 374 K. Representation by improved EOS mixing rules. Fluid Phase Equilibria. 1996;124:177-207.
81. Urlic LE, Florusse LJ, Straver EJM, Degrange S, Peters CJ. Phase and Interfacial Tension Behavior of Certain Model Gas Condensates: Measurements and Modeling. Transport in Porous Media. 2003;52:141-157.
82. Gozalpour F, Danesh A, Todd AC, Tehrani DH, Tohidi B. Vapour–liquid equilibrium volume and density measurements of a five-component gas condensate at 278.15–383.15 K. Fluid Phase Equilibria. 2003;206:95-104.
83. Jensen MR, Ungerer P, de Weert B, Behar E. Crystallisation of heavy hydrocarbons from three synthetic condensate gases at high pressure. Fluid Phase Equilibria. 2003;208:247-260.

Table 1: Experimental binary VLE data of CH_4 - *n*-alkane mixtures examined in this work.

Temperature (K)	Pressure (MPa)	Ref
CH_4 - *n*-$C_{10}H_{22}$		
244.26 – 277.59	1.56 – 6.90	59
263.15 – 303.15	1.60 – 36.53	60
310.90 – 410.90	1.04 – 8.65	61
423.15 – 583.05	3.04 – 18.68	62
237.15 – 423.15	0.053 – 10.13	63
310.93 – 510.93	0.14 – 36.20	64
293.15 – 472.47	11.30 – 35.98	65
CH_4 - *n*-$C_{12}H_{26}$		
263.15 – 303.15	1.41 – 49.48	66
323.2 – 373.2	1.33 – 10.38	61
374.05	9.97 – 40.79	67
CH_4 - *n*-$C_{16}H_{34}$		
290.00 – 360.00	2.15 – 70.35	68
293.15 – 313.15	2.09 – 69.55	69
303.20 – 323.20	0.06 – 0.51	70
324.00 – 413.20	7.60 – 31.90	71
462.45 – 703.55	2.05 – 25.26	72
623.10	2.50 – 18.00	73
CH_4 - *n*-$C_{20}H_{42}$		
313.15	0.10 – 6.08	74
323.20 – 423.20	0.95 – 10.69	75
323.15 – 353.15	0.41 – 83.40	76
373.35 – 573.15	1.01 – 5.05	77
CH_4 - *n*-$C_{24}H_{50}$		
325.00 – 425.00	1.93 – 104.05	78
373.15 – 573.15	1.01 – 5.07	79
374.05	20.10 – 84.30	80

Modeling the Phase Equilibria of Asymmetric Hydrocarbon Mixtures Using Molecular Simulation and Equations of State

Ilias K. Nikolaidis,[1,3] Ali Poursaeidesfahani,[2] Zsolt Csaszar,[2] Mahinder Ramdin,[2] Thijs J.H. Vlugt,[2] Ioannis G. Economou,[1,4] and Othonas A. Moultos[2,*]

[1]National Center for Scientific Research "Demokritos",
Institute of Nanoscience and Nanotechnology,
Molecular Thermodynamics and Modelling of Materials Laboratory,
GR – 153 10 Aghia Paraskevi Attikis, Greece

[2]Delft University of Technology,
Faculty of Mechanical, Maritime and Materials Engineering,
Process & Energy Department,
Engineering Thermodynamics,
Leeghwaterstraat 39, 2628CB Delft, The Netherlands

[3]National Technical University of Athens,
School of Chemical Engineering,
Heroon Polytechniou Street 9, Zografou Campus,
GR - 15780 Athens, Greece

[4]Texas A&M University at Qatar, Chemical Engineering Program, Education City,
PO Box 23874, Doha, Qatar

[*]corresponding author: o.moultos@tudelft.nl

Supporting Information

Cubic Equations of State

A general expression for a cubic Equation of State (EoS) is:[1]

$$P = \frac{RT}{v-b} - \frac{\alpha(T)}{(v+\delta_1 b)(v+\delta_2 b)} \tag{A1}$$

where R is the gas constant and $\alpha(T)$ and b are component-specific parameters that account for the attractive intermolecular interactions and the excluded volume of the component, respectively. In this study, these parameters are calculated based on the critical temperature (T_c), the critical pressure (P_c) and the acentric factor (ω) of the pure compound. For $\delta_1 = 1$ and $\delta_2 = 0$, eq. A1 takes the form of the SRK EoS, while for $\delta_1 = 1 + \sqrt{2}$ and $\delta_2 = 1 - \sqrt{2}$, the PR EoS is retrieved.

The van der Waals one fluid theory (vdW1f) mixing rules, using only one temperature-independent binary interaction parameter (k_{ij}) in the attractive term, are presented below:

$$\alpha = \sum_{i=1}^{C}\sum_{j=1}^{C} x_i x_j \alpha_{ij} \qquad \alpha_{ij} = \sqrt{\alpha_{ii}\alpha_{jj}}(1 - k_{ij}) \tag{A2}$$

$$b = \sum_{i=1}^{C} x_i b_i \tag{A3}$$

where x_i and x_j are the mole fractions of components i and j in a mixture of C components, respectively.

PC-SAFT Equation of State

Statistical Associating Fluid Theory (SAFT) based models are theoretically derived EoS based on rigorous perturbation theory.[2-4] Many versions of SAFT have been proposed in the literature, which differ mainly in the intermolecular potential used to model the reference fluid, all using the common framework of expressing the contributions of different molecular interactions as Helmholtz free energy terms. In this way, the total Helmholtz free energy of a fluid can be calculated as the sum of the individual contributions. Following this formulation, PC-SAFT is commonly written as summation of Helmholtz free energy terms:

$$\frac{A^{RESIDUAL}}{Nk_BT} = \frac{A^{HARD-CHAIN}}{Nk_BT} + \frac{A^{DISPERSION}}{Nk_BT} + \frac{A^{ASSOCIATION}}{Nk_BT} \tag{A4}$$

$$\frac{A^{HARD-CHAIN}}{Nk_BT} = \frac{A^{HARD-SPHERE}}{Nk_BT} + \frac{A^{CHAIN}}{Nk_BT} \tag{A5}$$

where A is the Helmholtz free energy and the superscripts refer to the respective molecular interaction contributions; N is the number of molecules and k_B is the Boltzmann constant. The reader can refer to the original publications[5,6] for the exact mathematical relations.

The vdW1f mixing rules as proposed by Gross and Sadowski,[5] with the adopted combining rules (Lorentz – Berthelot-based with a BIP incorporated into the Berthelot rule) are presented:

$$\overline{m^2 \frac{\varepsilon}{k_BT}\sigma^3} = \sum_{i=1}^{C}\sum_{j=1}^{C} x_i x_j m_i m_j \left[\frac{\varepsilon_{ij}}{k_BT}\right]\sigma_{ij}^3 \tag{A6}$$

$$\overline{m^2\left[\frac{\varepsilon}{k_B T}\right]^2 \sigma^3} = \sum_{i=1}^{C}\sum_{j=1}^{C} x_i x_j m_i m_j \left[\frac{\varepsilon_{ij}}{k_B T}\right]^2 \sigma_{ij}^3$$

$$\varepsilon_{ij} = \sqrt{\varepsilon_{ii}\varepsilon_{jj}}\left(1 - k_{ij}\right) \qquad \text{(A7)}$$

$$\sigma_{ij} = \frac{\sigma_{ii} + \sigma_{jj}}{2}$$

where m_i is the number of spherical segments in component i, ε_{ii} is the dispersion energy between spherical segments of component i and σ_{ii} is the temperature-independent diameter of each spherical segment in component i.

Monte Carlo Simulation Details

Advanced simulation techniques such as CBMC[7-9] or CFCMC[10,11] can be used to increase the acceptance probability of the molecule exchange trial move in MC simulations. In CFCMC, the interactions of a fractional molecule are scaled with a scaling parameter, λ, and molecules are gradually inserted / removed, allowing the surrounding molecules to adapt their configuration. A recent formulation of CFCMC by Poursaeidesfahni et al.[12,13] allows for the direct calculation of the chemical potential of all components, which can be used to verify the chemical equilibrium between the two phases. It should be noted that simulations in the Gibbs ensemble using CBMC or CFCMC or no advanced methods lead to identical results.[40,41,14] Simulations using CBMC are more straight forward and easier to manage, especially when a large number of simulations, for various mixtures at several conditions should be performed. However, at high densities the conventional methods for calculating the

chemical potential using CBMC might fail.[41,14] Contrary to CBMC, CFCMC simulations do not rely on occurrence of spontaneous cavities and therefore, have higher acceptance probabilities for the molecule exchange trial moves.

The TraPPE united atom (TraPPE-UA) force field was used for all the *n*-alkanes.[15] In the TraPPE-UA, CH_4, CH_3 and CH_2 groups are modeled as pseudo-atoms with no charges. The non-bonded intra- and intermolecular interactions between the pseudo-atoms are represented by the 12-6 Lennard-Jones (LJ) potential:

$$u_{nb}(r_{ij}) = 4\varepsilon_{ij}\left[\left(\frac{\sigma_{ij}}{r_{ij}}\right)^{12} - \left(\frac{\sigma_{ij}}{r_{ij}}\right)^{6}\right] \tag{A8}$$

where $\varepsilon_{ij}, \sigma_{ij}$ and r_{ij} are LJ energy parameter, the LJ size parameter and the distance between pseudoatoms *i* and *j*, respectively. In the TraPPE-UA, the intramolecular 1-4 interactions are excluded. The interactions between dissimilar pseudoatoms were described by the Lorentz-Berthelot mixing rules.[16] As required by the TraPPE-UA force field, the Lennard-Jones (LJ) interactions were truncated at 14 Å and analytic tail corrections were applied. Bond lengths are fixed to 1.54 Å. The bond-angle bending and torsional potentials are calculated from:

$$u_{bend}(\theta) = 31250k_B(\theta - 114)^2 \tag{A9}$$

$$\begin{aligned} u_{torsion}(\varphi) = k_B(&335.03[1 + cos\,\varphi] - 68.19[1 - cos\,2\varphi] \\ &+ 791.32[1 + cos\,3\varphi]) \end{aligned} \tag{A10}$$

where θ and φ are the bond-angle and dihedral angle, respectively.

Initially 50,000 Monte Carlo cycles were performed in every simulation to equilibrate the system, followed by 600,000 production cycles. The number of Monte Carlo steps per cycle equals the total number of molecules initially in the system, with a minimum of 20. The system size used was in the range of 500 – 1200 CH_4 molecules in total (in liquid and vapor phase) and 200 – 500 long *n*-alkanes molecules in total. These ranges correspond to simulation boxes of 40 – 50 Å for the liquid phase and 90 – 100 Å for the vapor phase. The total production run was divided into five blocks and the standard deviation of the block average was used for the calculation of the error in computed properties.

Table S1: Critical Temperature (T_c), Critical Pressure (P_c) and Acentric Factor (ω) values for the components studied in this work.

Component	T_c(K)	P_c(MPa)	ω	Ref
CH_4	190.564	4.599	0.0115	17
C_3H_8	369.830	4.248	0.1523	17
n-C_4H_{10}	425.120	3.796	0.2002	17
i-C_5H_{12}	460.430	3.381	0.2275	17
n-C_5H_{12}	469.700	3.370	0.2515	17
n-C_6H_{14}	507.600	3.025	0.3013	17
n-C_8H_{18}	568.700	2.490	0.3996	17
n-$C_{10}H_{22}$	617.700	2.110	0.4923	17
n-$C_{12}H_{26}$	658.000	1.820	0.5764	17
n-$C_{16}H_{34}$	723.000	1.400	0.7174	17
n-$C_{20}H_{42}$	768.000	1.160	0.9069	17
n-$C_{24}H_{50}$	804.000	0.980	1.0710	17

Table S2: PC-SAFT EoS parameters for the components studied in this work.

Component	m	σ(Å)	ε/k_B(K)	Ref
CH_4	1.0000	3.7039	150.03	5
C_3H_8	2.0020	3.6184	208.11	5
n-C_4H_{10}	2.3316	3.7086	222.88	5
i-C_5H_{12}	2.5620	3.8296	230.75	5
n-C_5H_{12}	2.6896	3.7729	231.20	5
n-C_6H_{14}	3.0576	3.7983	236.77	5
n-C_8H_{18}	3.8176	3.8373	242.78	5
n-$C_{10}H_{22}$	4.6627	3.8384	243.87	5
n-$C_{12}H_{26}$	5.3060	3.8959	249.21	5
n-$C_{16}H_{34}$	6.6485	3.9552	254.70	5
n-$C_{20}H_{42}$	7.9849	3.9869	257.75	5
n-$C_{24}H_{50}$	9.6836	3.9709	254.69	18

Table S3: CH_4 - n-$C_{10}H_{22}$ mixture Gibbs Ensemble Monte Carlo simulation data. The statistical uncertainty in the last digit is given in parentheses (i.e., 0.503(3) is 0.503±0.003).

Temperature (K)	Pressure (MPa)	CH_4 mole fraction liquid phase	CH_4 mole fraction vapor phase
244	10.01	0.503(3)	0.997(1)
244	15.02	0.59(1)	0.997(1)
244	19.97	0.66(2)	0.992(2)
244	25.05	0.72(3)	0.984(2)
244	30.03	0.76(2)	0.973(3)
244	35.02	0.81(2)	0.95(1)
255	1.00	0.065(3)	0.962(1)
255	9.99	0.464(5)	0.9971(1)
255	25.05	0.72(1)	0.988(3)
255	30.02	0.77(1)	0.976(4)
255	34.98	0.81(1)	0.957(6)
277	0.99	0.054(3)	0.962(1)
277	5.03	0.244(8)	0.9926(1)
277	10.03	0.42(1)	0.9966(2)
277	20.03	0.628(5)	0.992(1)
277	25.00	0.70(1)	0.985(1)
277	30.02	0.75(3)	0.97(1)
277	35.02	0.80(2)	0.96(2)
283	1.00	0.051(2)	0.961(1)
283	5.01	0.242(3)	0.9923(1)
283	10.01	0.40(1)	0.9966(1)
283	13.60	0.502(6)	0.9985(1)
283	17.39	0.577(1)	0.9962(6)
283	24.07	0.68(1)	0.984(5)
283	30.04	0.75(3)	0.96(1)
283	34.97	0.81(4)	0.96(2)
303	1.00	0.048(2)	0.960(1)
303	5.07	0.221(4)	0.9918(1)
303	10.03	0.380(2)	0.9962(1)
303	14.86	0.501(5)	0.9973(2)
303	25.13	0.67(1)	0.98(1)
303	31.49	0.77(4)	0.95(2)

310	1.00	0.045(2)	0.958(1)
310	4.97	0.212(6)	0.9915(2)
310	15.52	0.505(3)	0.9965(4)
310	17.27	0.541(5)	0.9956(7)
310	18.96	0.571(6)	0.9937(6)
310	20.66	0.603(7)	0.991(1)
310	22.47	0.63(1)	0.989(2)
310	24.17	0.65(1)	0.98(1)
310	25.82	0.68(1)	0.979(6)
310	27.53	0.71(1)	0.96(1)
310	29.26	0.73(1)	0.95(1)
310	32.77	0.78(1)	0.94(2)
310	34.45	0.8(1)	0.95(5)
450	4.99	0.167(5)	0.948(4)
450	9.97	0.308(3)	0.956(2)
450	14.99	0.433(3)	0.950(1)
450	19.95	0.544(3)	0.933(4)
450	24.97	0.73(4)	0.84(4)
550	5.02	0.156(3)	0.652(2)
550	9.98	0.40(7)	0.659(8)
550	11.07	0.47(8)	0.655(9)
550	13.01	0.56(6)	0.65(4)

Table S4: CH_4 - n-$C_{12}H_{26}$ mixture Gibbs Ensemble Monte Carlo simulation data. The statistical uncertainty in the last digit is given in parentheses.

Temperature (K)	Pressure (MPa)	CH_4 mole fraction liquid phase	CH_4 mole fraction vapor phase
283	1.00	0.056(4)	0.961(1)
283	5.02	0.242(6)	0.9927(1)
283	9.99	0.398(7)	0.9967(1)
283	15.03	0.51(1)	0.9979(1)
283	21.03	0.606(8)	0.997(2)
283	29.46	0.701(9)	0.98(1)
283	35.39	0.76(3)	0.98(2)
303	1.00	0.051(5)	0.960(2)
303	5.03	0.223(4)	0.9921(1)
303	10.04	0.37(1)	0.9963(1)
303	21.95	0.606(4)	0.996(1)
303	30.03	0.705(8)	0.988(3)
303	35.27	0.75(1)	0.983(4)
303	40.24	0.82(3)	0.971(5)
323	1.00	0.045(3)	0.958(1)
323	4.98	0.206(4)	0.9914(1)
323	9.98	0.354(7)	0.9959(1)
323	20.01	0.560(5)	0.997(2)
323	24.99	0.632(5)	0.994(6)
323	30.04	0.69(1)	0.98(1)
323	34.96	0.75(1)	0.97(2)
323	40.00	0.81(2)	0.96(1)
373	1.01	0.039(1)	0.9523(8)
373	5.02	0.184(2)	0.9900(1)
373	9.98	0.325(4)	0.9951(1)
373	15.01	0.442(3)	0.9962(3)
373	20.00	0.536(3)	0.9935(3)
373	25.02	0.615(4)	0.9892(8)
373	30.05	0.683(6)	0.981(1)
373	35.00	0.75(2)	0.96(1)
373	40.00	0.85(4)	0.92(3)
400	5.00	0.181(3)	0.9955(5)

400	10.00	0.314(5)	0.9948(5)
400	15.00	0.433(2)	0.9934(5)
400	20.00	0.524(5)	0.9895(7)
400	25.00	0.608(7)	0.983(1)
400	30.00	0.68(1)	0.971(5)
400	32.00	0.72(2)	0.964(5)
400	35.00	0.78(2)	0.93(1)
400	37.00	0.82(4)	0.91(3)
450	5.00	0.1717	0.9811
450	10.00	0.3119	0.9830
450	15.00	0.4311	0.9813
450	20.00	0.5241	0.9738
450	25.00	0.6094	0.9591
450	26.00	0.637(2)	0.960(2)
450	28.00	0.669(7)	0.949(4)
500	1.04	0.033(1)	0.79(1)
500	5.00	0.170(3)	0.942(2)
500	10.00	0.312(4)	0.952(2)
500	15.00	0.43(1)	0.947(5)
500	20.00	0.53(1)	0.933(7)
500	21.00	0.573(3)	0.933(2)
500	23.00	0.611(1)	0.923(1)
500	25.00	0.67(7)	0.89(2)
550	0.99	0.021(1)	0.46(2)
550	2.00	0.061(2)	0.70(1)
550	5.00	0.167(2)	0.84(1)
550	8.00	0.263(5)	0.876(5)
550	10.00	0.327(8)	0.88(1)
550	15.00	0.45(7)	0.85(4)
550	16.00	0.50(4)	0.83(2)
550	17.00	0.56(6)	0.79(5)
550	18.00	0.60(2)	0.75(2)
550	19.00	0.64(2)	0.68(4)
600	1.05	0.0056(1)	0.067(2)
600	2.54	0.073(2)	0.45(2)

600	5.11	0.210(5)	0.50(3)

Table S5: CH_4 - *n*-$C_{16}H_{34}$ mixture Gibbs Ensemble Monte Carlo simulation data. The statistical uncertainty in the last digit is given in parentheses.

Temperature (K)	Pressure (MPa)	CH_4 mole fraction liquid phase	CH_4 mole fraction vapor phase
340	0.99	0.049(5)	1.0000(1)
340	4.98	0.210(5)	1.0000(1)
340	10.01	0.359(2)	1.0000(1)
340	15.03	0.463(8)	0.9971(1)
340	19.97	0.545(5)	0.9978(1)
340	24.56	0.602(2)	0.9984(1)
340	36.42	0.719(4)	0.9943(2)
340	53.30	0.85(1)	0.9697(5)
400	1.00	0.042(3)	0.9490(4)
400	4.98	0.186(3)	0.9890(1)
400	10.01	0.329(3)	0.9945(5)
400	15.02	0.436(5)	0.9964(3)
400	20.04	0.5243(6)	0.9973(2)
400	30.06	0.659(5)	0.9947(1)
462	2.08	0.083(1)	0.9934(1)
462	5.09	0.186(2)	0.9960(1)
462	10.29	0.331(2)	0.9960(1)
462	14.96	0.433(4)	0.9949(1)
462	20.08	0.526(7)	0.9928(4)
462	25.58	0.61(2)	0.989(2)
500	1.00	0.039(2)	0.952(1)
500	4.98	0.182(3)	0.9896(1)
500	9.95	0.323(3)	0.9900(1)
500	15.09	0.440(4)	0.988(1)
500	19.96	0.532(3)	0.9855(1)
500	29.95	0.683(4)	0.972(1)
500	35.00	0.77(2)	0.94(1)
550	1.00	0.0384(3)	0.878(6)

550	4.98	0.184(1)	0.963(1)
550	9.97	0.331(3)	0.971(1)
550	15.07	0.451(6)	0.968(3)
550	20.05	0.556(5)	0.963(3)
600	1.00	0.0323(7)	0.65(1)
600	4.98	0.190(3)	0.901(4)
600	9.96	0.348(1)	0.927(3)
600	14.97	0.48(1)	0.91(2)
600	20.02	0.69(7)	0.86(4)
623	2.14	0.079(1)	0.731(2)
623	3.23	0.126(2)	0.81(1)
623	5.13	0.207(3)	0.86(1)
623	10.03	0.38(2)	0.87(2)
670	1.00	0.012(2)	0.14(1)
670	3.00	0.107(1)	0.531(9)
670	5.02	0.202(3)	0.66(2)
670	6.98	0.30(3)	0.71(3)

Table S6: CH_4 - *n*-$C_{20}H_{42}$ mixture Gibbs Ensemble Monte Carlo simulation data. The statistical uncertainty in the last digit is given in parentheses.

Temperature (K)	Pressure (MPa)	CH_4 mole fraction liquid phase	CH_4 mole fraction vapor phase
323	1.01	0.06(1)	1.0000(1)
323	5.02	0.25(1)	1.0000(1)
323	10.00	0.399(8)	0.9954(1)
323	15.02	0.50(1)	0.9970(1)
323	20.02	0.575(1)	0.9978(1)
323	25.01	0.62(1)	0.9982(1)
323	34.95	0.70(1)	0.9978(1)
323	39.99	0.73(1)	0.9980(1)
323	44.94	0.76(1)	0.9963(1)
323	62.76	0.83(1)	0.9892(4)
323	71.42	0.863(8)	0.9839(4)
323	79.87	0.91(2)	0.9674(4)

323	83.20	0.931(1)	0.956(6)
323	83.41	0.934(4)	0.953(3)
353	1.00	0.051(2)	0.9505(3)
353	4.99	0.22(1)	0.9896(1)
353	10.01	0.369(8)	0.9950(1)
353	14.98	0.47(1)	0.9967(1)
353	20.00	0.550(6)	0.9975(1)
353	24.99	0.611(7)	0.9980(1)
353	29.98	0.659(9)	0.9974(1)
353	35.04	0.701(3)	0.9977(1)
353	40.08	0.730(2)	0.9959(1)
353	45.11	0.765(8)	0.9945(4)
353	58.92	0.84(2)	0.987(1)
353	66.07	0.86(1)	0.982(1)
353	72.88	0.90(2)	0.968(6)
353	75.40	0.92(1)	0.960(4)
423	15.01	0.447(2)	0.9959(1)
423	20.05	0.533(2)	0.9969(1)
423	25.02	0.598(3)	0.9975(2)
423	35.08	0.706(5)	0.9973(4)
423	44.94	0.779(6)	0.992(2)
423	50.08	0.81(1)	0.987(3)
423	55.00	0.84(1)	0.978(5)
423	60.01	0.87(1)	0.970(1)
500	0.99	0.042(2)	0.9391(1)
500	5.04	0.195(4)	0.985(1)
500	10.07	0.336(6)	0.9928(2)
500	14.96	0.449(5)	0.9968(4)
500	20.05	0.53(1)	0.9956(6)
500	25.01	0.612(4)	0.9940(6)
500	30.07	0.67(1)	0.991(1)
500	34.96	0.728(8)	0.987(3)
500	40.05	0.780(8)	0.983(2)
500	45.04	0.83(2)	0.95(1)
550	1.00	0.043(2)	0.926(2)

550	5.05	0.199(5)	0.9848(1)
550	10.10	0.346(4)	0.9921(2)
550	14.93	0.462(5)	0.9908(4)
550	20.07	0.55(1)	0.9875(6)
550	25.07	0.629(4)	0.9847(6)
550	30.04	0.69(1)	0.977(1)
550	35.03	0.788(7)	0.952(3)
600	0.99	0.043(1)	0.890(8)
600	5.04	0.207(2)	0.969(8)
600	10.08	0.361(5)	0.975(2)
600	15.11	0.485(6)	0.975(1)
600	20.07	0.579(5)	0.970(1)
600	24.98	0.666(3)	0.962(4)
650	5.00	0.212(1)	0.917(2)
650	8.00	0.316(3)	0.935(1)
650	10.00	0.373(2)	0.935(1)
650	12.00	0.428(7)	0.94(1)
650	15.00	0.49(3)	0.93(1)
700	1.00	0.027(1)	0.35(1)
700	5.11	0.227(3)	0.78(1)
700	10.05	0.416(5)	0.83(1)
700	12.04	0.57(9)	0.79(1)

Table S7: CH_4 - *n*-$C_{24}H_{50}$ mixture Gibbs Ensemble Monte Carlo simulation data. The statistical uncertainty in the last digit is given in the parentheses.

Temperature (K)	Pressure (MPa)	CH_4 mole fraction liquid phase	CH_4 mole fraction vapor phase
330	10.02	0.43(1)	1.0000
330	15.01	0.52(2)	1.0000
330	20.00	0.597(5)	1.0000
330	30.03	0.68(1)	1.0000
330	35.01	0.71(1)	1.0000
330	40.04	0.73(1)	1.0000
330	44.97	0.76(1)	1.0000

330	49.96	0.78(2)	1.0000
330	59.55	0.817(4)	0.9951(1)
330	69.51	0.84(2)	0.9924(7)
330	83.10	0.88(1)	0.9870(6)
330	97.09	0.93(1)	0.965(5)
350	5.01	0.26(2)	1.0000
350	10.02	0.41(1)	1.0000
350	15.02	0.50(1)	1.0000
350	19.99	0.57(1)	1.0000
350	25.01	0.62(1)	1.0000
350	29.96	0.67(1)	1.0000
350	35.05	0.71(1)	1.0000
350	39.96	0.740(6)	1.0000
350	45.00	0.76(1)	1.0000
350	57.29	0.81(1)	0.9949(2)
350	66.08	0.84(1)	0.9920(6)
350	78.04	0.88(1)	0.986(1)
350	90.14	0.94(1)	0.965(13)
374	0.90	0.060(1)	1.0000
374	5.05	0.242(6)	1.0000
374	10.02	0.38(1)	1.0000
374	15.01	0.48(1)	1.0000
374	19.98	0.56(1)	1.0000
374	25.02	0.62(1)	1.0000
374	30.00	0.67(1)	1.0000
374	35.00	0.70(1)	1.0000
374	39.97	0.736(8)	1.0000
374	45.04	0.765(5)	1.0000
374	49.98	0.79(1)	1.0000
374	55.15	0.815(6)	0.9946(4)
374	60.17	0.837(7)	0.9930(1)
374	71.07	0.873(7)	0.9874(3)
374	80.21	0.914(8)	0.976(6)
374	84.30	0.94(1)	0.963(4)
400	4.99	0.22(1)	0.9130(1)

400	10.04	0.393(6)	0.9323(2)
400	15.02	0.50(1)	0.9336(2)
400	19.97	0.570(6)	0.9504(4)
400	25.04	0.622(6)	0.962(1)
400	30.02	0.673(3)	0.9658(5)
400	35.03	0.71(1)	0.972(1)
400	40.07	0.74(1)	0.979(4)
400	45.04	0.77(1)	0.994(3)
400	50.01	0.797(6)	0.992(1)
400	55.06	0.835(4)	0.9898(6)
450	10.00	0.343(1)	0.9950(5)
450	20.00	0.544(3)	0.9983(1)
450	30.00	0.652(4)	0.9972(2)
450	40.00	0.74(1)	0.9911(1)
450	50.00	0.83(2)	0.9575(1)
500	0.98	0.048(2)	0.9983(1)
500	10.05	0.35(1)	0.9992(1)
500	15.03	0.46(1)	0.9990(1)
500	20.12	0.55(1)	0.9983(2)
500	25.03	0.62(1)	0.9977(3)
500	30.08	0.677(7)	0.996(1)
500	35.03	0.72(1)	0.995(1)
500	40.10	0.77(1)	0.992(3)
500	45.02	0.806(7)	0.987(5)
500	50.02	0.84(2)	0.97(1)
550	5.00	0.213(2)	0.9971(1)
550	10.00	0.36(1)	0.9973(1)
550	20.00	0.564(7)	0.9581(2)
550	30.00	0.694(4)	0.9932(4)
550	35.00	0.74(1)	0.989(1)
600	1.04	0.050(7)	0.963(7)
600	10.21	0.377(6)	0.990(1)
600	15.05	0.494(4)	0.990(1)
600	19.99	0.588(6)	0.988(2)
600	25.07	0.661(4)	0.985(2)

600	30.05	0.733(8)	0.981(3)
700	1.03	0.047(1)	0.71(1)
700	5.22	0.249(6)	0.916(8)
700	10.17	0.423(3)	0.937(3)
700	15.01	0.549(7)	0.93(1)
750	1.08	0.038(3)	0.38(4)
750	5.01	0.255(4)	0.78(2)
750	7.40	0.37(2)	0.80(4)
750	9.98	0.52(9)	0.82(3)

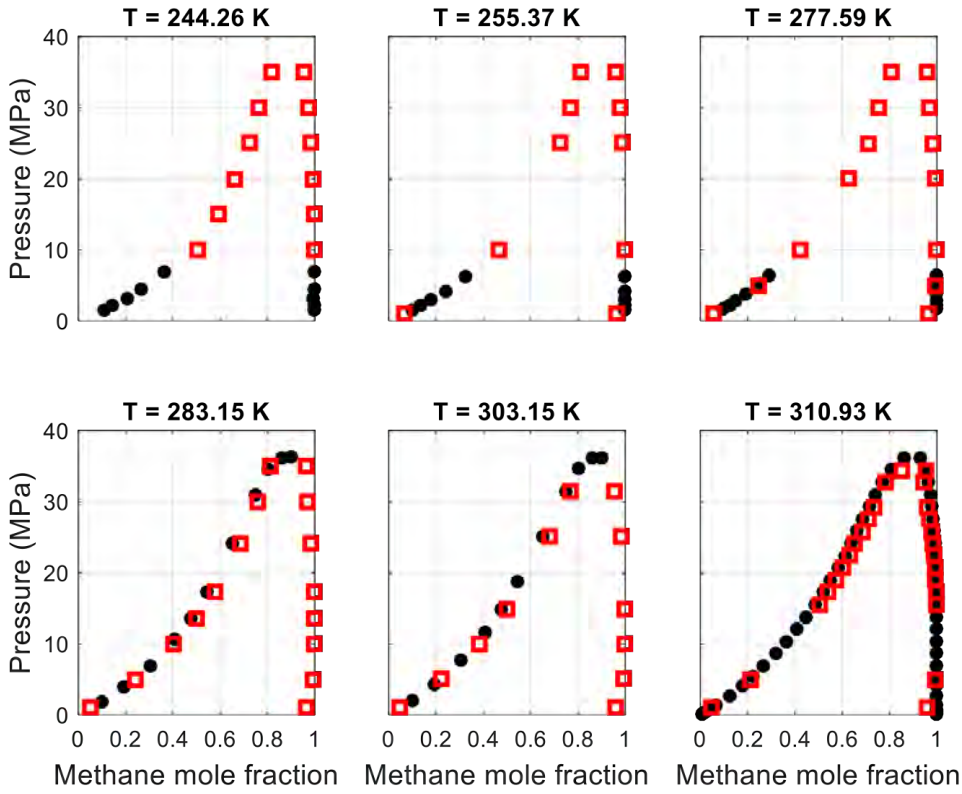

Figure S1: Pressure – composition VLE for the CH_4 - *n*-$C_{10}H_{22}$ mixture at various temperatures. Experimental data[19-21] are represented by black data points. GEMC simulation data are represented by red squares.

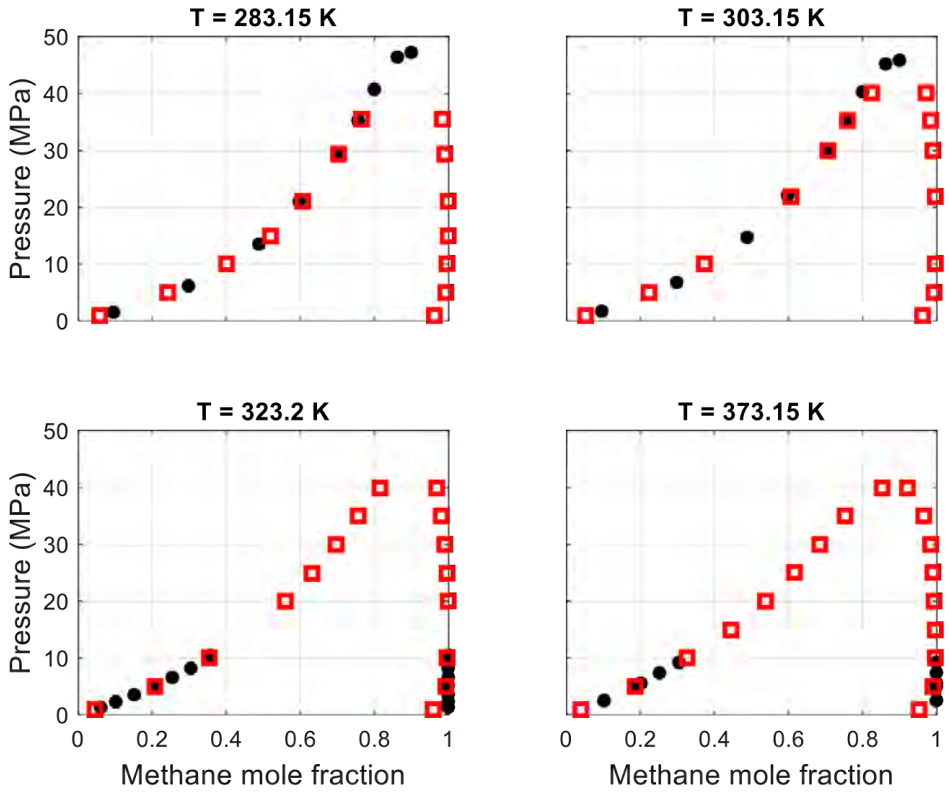

Figure S2: Pressure – composition VLE for the CH_4 - n-$C_{12}H_{26}$ mixture at various temperatures. Experimental data[22,23] are represented by black data points. GEMC simulation data are represented by red squares.

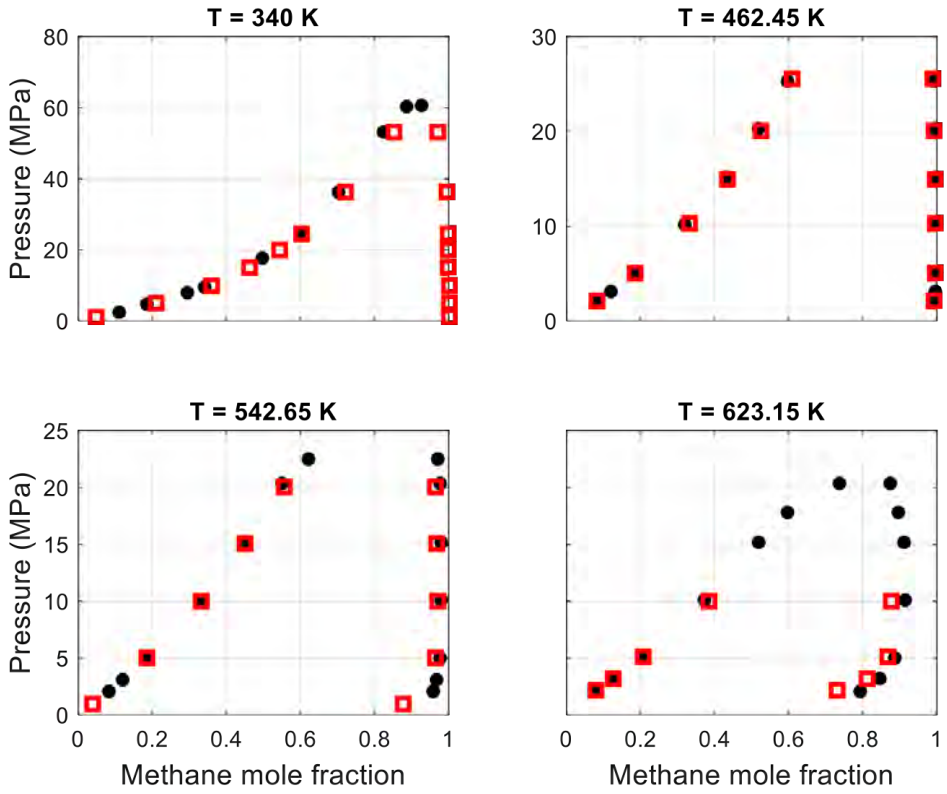

Figure S3: Pressure – composition VLE for the CH_4 - n-$C_{16}H_{34}$ mixture at various temperatures. Experimental data[24,25] are represented by black data points. GEMC simulation data are represented by red squares.

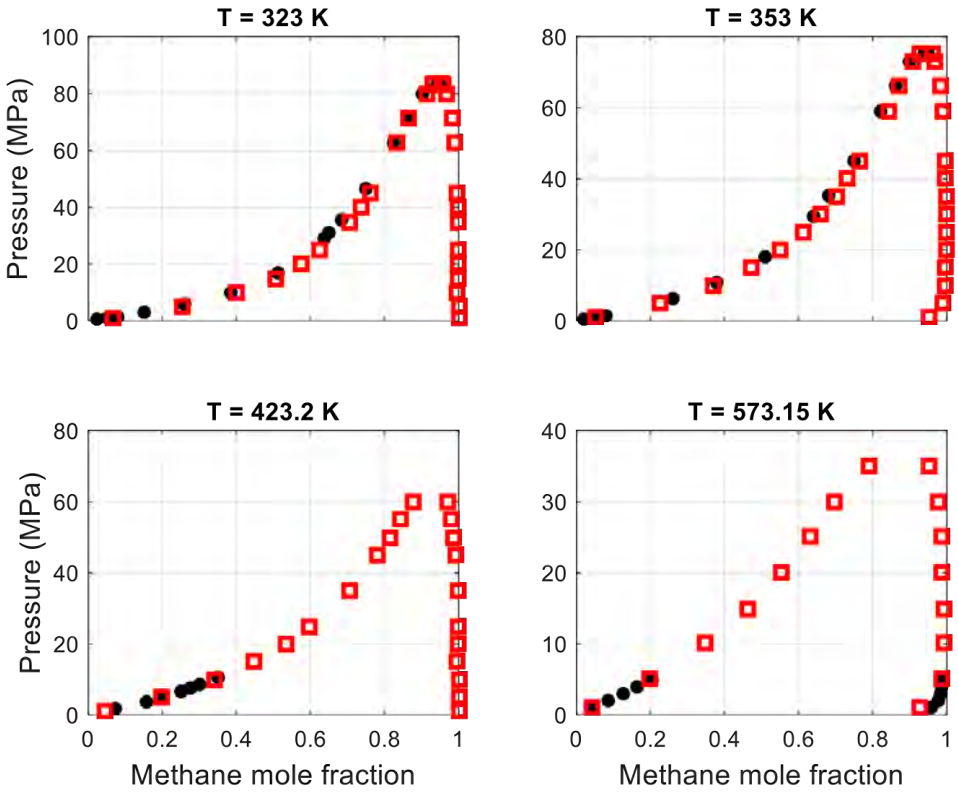

Figure S4: Pressure – composition VLE for the CH_4 - *n*-$C_{20}H_{42}$ mixture at various temperatures. Experimental data[26-28] are represented by black data points. GEMC simulation data are represented by red squares.

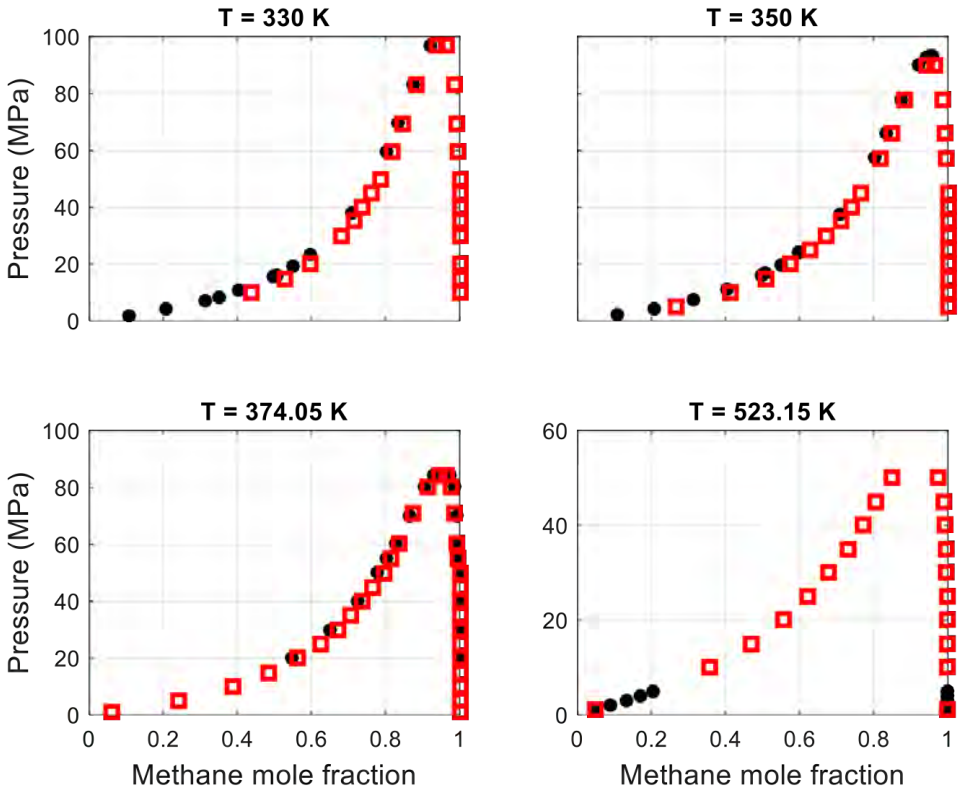

Figure S5: Pressure – composition VLE for the CH_4 - n-$C_{24}H_{50}$ mixture at various temperatures. Experimental data[29-31] are represented by black data points. GEMC simulation data are represented by red squares.

References

1. Michelsen ML, Mollerup JM. Thermodynamic Models: Fundamentals & Computational Aspects (2nd edition). Denmark: Tie-Line Publications, 2007.
2. Chapman WG, Gubbins KE, Jackson G, Radosz M. New reference equation of state for associating liquids. Industrial & Engineering Chemistry Research. 1990;29:1709-1721.
3. Chapman WG, Jackson G, Gubbins KE. Phase equilibria of associating fluids. Molecular Physics. 1988;65:1057-1079.
4. Jackson G, Chapman WG, Gubbins KE. Phase equilibria of associating fluids. Molecular Physics. 1988;65:1-31.
5. Gross J, Sadowski G. Perturbed-Chain SAFT: An Equation of State Based on a Perturbation Theory for Chain Molecules. Industrial & Engineering Chemistry Research. 2001;40:1244-1260.
6. Gross J, Sadowski G. Application of the Perturbed-Chain SAFT Equation of State to Associating Systems. Industrial & Engineering Chemistry Research. 2002;41:5510-5515.
7. Consta S, Vlugt TJH, Hoeth JW, Smit B, Frenkel D. Recoil growth algorithm for chain molecules with continuous interactions. Molecular Physics. 1999;97:1243-1254.
8. Siepmann JI. A method for the direct calculation of chemical potentials for dense chain systems. Molecular Physics. 1990;70:1145-1158.
9. Siepmann JI, Karaborni S, Smit B. Vapor-liquid equilibria of model alkanes. Journal of the American Chemical Society. 1993;115:6454-6455.
10. Shi W, Maginn EJ. Continuous Fractional Component Monte Carlo: An Adaptive Biasing Method for Open System Atomistic Simulations. Journal of Chemical Theory and Computation. 2007;3:1451-1463.
11. Shi W, Maginn EJ. Improvement in molecule exchange efficiency in Gibbs ensemble Monte Carlo: Development and implementation of the continuous fractional component move. Journal of Computational Chemistry. 2008;29:2520-2530.
12. Poursaeidesfahani A, Rahbari A, Torres-Knoop A, Dubbeldam D, Vlugt TJH. Computation of thermodynamic properties in the continuous fractional component Monte Carlo Gibbs ensemble. Molecular Simulation. 2017;43:189-195.
13. Poursaeidesfahani A, Torres-Knoop A, Dubbeldam D, Vlugt TJH. Direct Free Energy Calculation in the Continuous Fractional Component Gibbs Ensemble. Journal of Chemical Theory and Computation. 2016;12:1481-1490.
14. Rahbari A, Poursaeidesfahani A, Torres-Knoop A, Dubbeldam D, Vlugt TJH. Chemical potentials of water, methanol, carbon dioxide and hydrogen sulphide at low temperatures using continuous fractional component Gibbs ensemble Monte Carlo. Molecular Simulation. 2018;44:405-414.
15. Martin MG, Siepmann JI. Transferable Potentials for Phase Equilibria. 1. United-Atom Description of n-Alkanes. The Journal of Physical Chemistry B. 1998;102:2569-2577.
16. Allen MP, Tildesley DJ. Computer simulation of liquids New York: Oxford University Press, 1989.
17. DIPPR 801, Evaluated Standards Thermophysical Property Values. American Institute of Chemical Engineers; 2015.
18. MAPS; Materials and Processes Simiulations Platform, Version v4.0, Scienomics. SARL, Paris, France.
19. Koonce KT, Kobayashi R. A Method for Determining the Solubility of Gases in Relatively Nonvolatile Liquids: Solubility of Methane in n-Decane. Journal of Chemical & Engineering Data. 1964;9:490-494.
20. Rijkers MPWM, Malais M, Peters CJ, de Swaan Arons J. Measurements on the phase behavior of binary hydrocarbon mixtures for modelling the condensation behavior of natural gas: Part I. The system methane + decane. Fluid Phase Equilibria. 1992;71:143-168.
21. Reamer HH, Olds RH, Sage BH, Lacey WN. Phase Equilibria in Hydrocarbon Systems. Industrial & Engineering Chemistry. 1942;34:1526-1531.

22. Rijkers MPWM, Maduro VB, Peters CJ, de Swaan Arons J. Measurements on the phase behavior of binary mixtures for modeling the condensation behavior of natural gas: Part II. The system methane + dodecane. Fluid Phase Equilibria. 1992;72:309-324.
23. Srivastan S, Darwish NA, Gasem KAM, Robinson RL. Solubility of methane in hexane, decane, and dodecane at temperatures from 311 to 423 K and pressures to 10.4 MPa. Journal of Chemical & Engineering Data. 1992;37:516-520.
24. Glaser M, Peters CJ, Van Der Kooi HJ, Lichtenthaler RN. Phase equilibria of (methane + n-hexadecane) and (p, Vm, T) of n-hexadecane. The Journal of Chemical Thermodynamics. 1985;17:803-815.
25. Lin H-M, Sebastian HM, Chao K-C. Gas-liquid equilibrium in hydrogen + n-hexadecane and methane + n-hexadecane at elevated temperatures and pressures. Journal of Chemical & Engineering Data. 1980;25:252-254.
26. van der Kooi HJ, Flöter E, Loos TWd. High-pressure phase equilibria of {(1−x)CH4+xCH3(CH2)18CH3}. The Journal of Chemical Thermodynamics. 1995;27:847-861.
27. Darwish NA, Fathikalajahi J, Gasem KAM, Robinson RL. Solubility of methane in heavy normal paraffins at temperatures from 323 to 423 K and pressures to 10.7 MPa. Journal of Chemical & Engineering Data. 1993;38:44-48.
28. Huang SH, Lin HM, Chao KC. Solubility of carbon dioxide, methane, and ethane in n-eicosane. Journal of Chemical & Engineering Data. 1988;33:145-147.
29. Flöter E, de Loos TW, de Swaan Arons J. High pressure solid-fluid and vapour-liquid equilibria in the system (methane + tetracosane). Fluid Phase Equilibria. 1997;127:129-146.
30. Arnaud JF, Ungerer P, Behar E, Moracchini G, Sanchez J. Excess volumes and saturation pressures for the system methane + n-tetracosane at 374 K. Representation by improved EOS mixing rules. Fluid Phase Equilibria. 1996;124:177-207.
31. Huang C-P, Jan D-S, Tsai F-N. Modeling of Methane Solubility in Heavy n-Paraffins. Journal of Chemical Engineering of Japan. 1992;25:182-186.